**Wen-Tao Ji**[1]
Key Laboratory of Thermo-Fluid Science and Engineering of MOE,
School of Energy and Power Engineering,
Xi'an Jiaotong University,
Xi'an 710049, China
e-mail: wentaoji@xjtu.edu.cn

**Chuang-Yao Zhao**
Key Laboratory of Thermo-Fluid Science and Engineering of MOE,
School of Energy and Power Engineering,
Xi'an Jiaotong University,
Xi'an 710049, China

**Jessica Lofton**
Mechanical Engineering,
University of Evansville,
Evansville, IN 47722

**Zeng-Yao Li**
Key Laboratory of Thermo-Fluid Science and Engineering of MOE,
School of Energy and Power Engineering,
Xi'an Jiaotong University,
Xi'an 710049, China

**Ding-Cai Zhang**
Key Laboratory of Thermo-Fluid Science and Engineering of MOE,
School of Energy and Power Engineering,
Xi'an Jiaotong University,
Xi'an 710049, China

**Ya-Ling He**
Key Laboratory of Thermo-Fluid Science and Engineering of MOE,
School of Energy and Power Engineering,
Xi'an Jiaotong University,
Xi'an 710049, China

**Wen-Quan Tao**
Key Laboratory of Thermo-Fluid Science and Engineering of MOE,
School of Energy and Power Engineering,
Xi'an Jiaotong University,
Xi'an 710049, China

# Condensation of R134a and R22 in Shell and Tube Condensers Mounted With High-Density Low-Fin Tubes

*In this work, the condensation of refrigerants on a single, high-density, low-fin tube and full-sized shell and tube condensers were investigated experimentally. The low-fin tube had an external fin density of 56 fins per inch (fpi) and fin height 1.023 mm. Another three-dimensional (3D) finned tube was also tested for comparison. The condensing heat transfer coefficient of the refrigerant R134a was first investigated outside a single horizontal tube at saturation temperature of 40 °C. The overall heat transfer coefficients of the two tubes were similar in magnitude. The condensing heat transfer coefficient of the low-fin tube was 16.3–25.2% higher than that of 3D enhanced tube. The experiments of the two condensers mounted with low-fin and 3D enhanced tubes were then conducted in centrifugal and screw chiller test rigs. It was found that chillers with the two different condensers generally had the same refrigeration capacity under the same experiment conditions. The refrigeration capacity of the screw chiller was smaller. It had fewer tube rows and elicited fewer inundation effects owing to the falling condensate. The heat transfer coefficients of the condensers with R134a in centrifugal chillers equipped with high-density low-finned tubes were higher than those in the screw chillers. The total number of tubes for low-fin tube condensers, in the two chillers, was reduced by approximately 15% compared with the use of domestic advanced condensers equipped with the 3D enhanced tubes.* [DOI: 10.1115/1.4040083]

*Keywords: condensation, heat transfer, tube, chiller*

## 1 Introduction

Shell and tube condenser might be the most common types of heat exchangers used in the refrigeration and air-conditioning industry. In the condensers, cooling water flows through the tube side while refrigerant vapor at medium pressure is passing over the external surface of tube bundle. Condensation occurs outside the horizontal tubes. The water can be in a closed loop with a cooling tower. They have a cooling capacity that ranges from 10 to 10 MW or more. The shell cylinder's diameter ranges from approximately 200 mm to 2 m. In consideration of the energy and materials savings, many types of enhanced tubes have been developed [1–5]. The inner and outer surfaces have been manufactured with different types of fins to minimize the material consumption and reduce the condenser or evaporator size [6–13]. A number of double sided enhanced tubes are now practically and commercially available, such as Thermoexcel-C (Hitachi), Turbo-C (Wolverine), and GEWA-C5 (Wieland), which typically have sharp fins to reduce the condensate film thickness. Normally, the enhanced tubes used for condensing heat transfer enhancement include integral low-fin, and three-dimensional (3D) finned tubes.

Integral low-fin tubes have been used in the heat exchangers since the 1940s [14]. They also yielded a higher heat transfer coefficient for condensation, especially that with slim fins. At the early stages, the heat transfer was supposed to be enhanced by increased

[1]Corresponding author.

Contributed by the Heat Transfer Division of ASME for publication in the Journal of Heat Transfer. Manuscript received May 15, 2017; final manuscript received April 12, 2018; published online May 25, 2018. Assoc. Editor: Amitabh Narain.

  

surface area. The effect of surface tension on the film condensation outside the finned surface was first recognized by Gregorig [15]. The effect of surface tension could be a dominant force for pulling the condensate into concave grooves, thus reducing the liquid film thickness along the tube circumference. Thinner film thickness led to higher condensing heat transfer coefficient. According to the research of Webb and coworkers [16,17], the fin efficiency could be further improved by reducing the fin thickness. Increase of fin height also had a favorable effect on condensing heat transfer because the film thickness in the fin tips could be further reduced under the effect of surface tension.

Advanced manufacturing techniques led to the development of three-dimensional fin profiles, fabricated by cutting or plowing on the two-dimensional grooves. The small sharp tips separating the grooves aided not only in forming thin film outside the fin tips but also dividing the liquid films into pieces. Separating the liquid film exposed more effective condensing surfaces to vapor and allowed rapid drainage of condensate into grooves. Enhanced tubes with 3D fin profiles are widely used in water-cooled chillers. While 3D enhanced tubes' performance might decrease in a tube row because of row effect [17,18], low-fin tube mostly showed virtually no row effect.

The row effect of three-dimensional enhanced and low-fin tubes has been investigated in previous studies. Webb and Murawski [17] tested the condensing heat transfer of refrigerant R11 on a vertical row of five horizontal tubes. The tubes included low-fin tube with fin density of 26 fpi and 3D enhanced tubes: Turbo-C, GEWA-SC, and Tred-D. Film Reynolds number ranged from 200 to 1000. The low-fin tube results demonstrated that row effect was negligible. The average condensation heat transfer coefficient for the entire tube bundle decreased at least 27% for GEWA-SC tube, whereas a decrease greater than 100% was observed for Turbo-C tube. At film Reynolds numbers greater than 600, only GEWA-SC tube provided an average condensation coefficient comparable to that of the low-fin tube. It was speculated that the beneficial row effect of low-fin tubes was because the continuous fins might act as dams, which blocked the axial spreading of film condensate.

Film condensation of R-113 on the staggered bundles with different enhanced tubes was investigated by Honda et al. [19]. The tube bundle had three columns and 15 rows in the gas flow direction. Two low-fin tubes (with fin densities of 27 and 51 fpi) and four 3D finned tubes were tested. The longitudinal and transverse tube pitches were both equal to 22 mm. Experimental results revealed the differences in the relationship between Nusselt number and film Reynolds number for low-fin and 3D fin tubes. For low-fin tube, the condensing heat transfer coefficient was relatively insensitive to the film's Reynolds number, whereas the Nusselt number decreased abruptly with increasing Reynolds numbers in the case of 3D enhanced tubes. It was speculated that the longitudinal grooves between the three-dimensional fins might act to equalize the condensate along the tube length and retain the condensate within the fins. The effective condensing surface area decreased for the 3D enhanced tube at higher film Reynolds numbers.

Cheng and Wang [20] tested the condensing heat transfer of R134a on a vertical column of horizontal enhanced tubes. One plain tube, three low-fin tubes (26 fpi, 32 fpi and 41 fpi), and three three-dimensional enhanced tubes were tested. The inline vertical row had three tubes. It was found that low-fin tubes showed almost no measurable variations of the heat transfer coefficient with row number. However, the heat transfer coefficient exhibited a noticeable decay for increasing row number with 3D enhanced tubes. The condensing heat transfer coefficient decreased by approximately 20% for 3D finned tubes when the row number increased from 1 to 3.

Gstoehl and Thome experimentally investigated the film condensation of R134a outside one low-fin and two 3D enhanced tubes [21,22]. The 3D enhanced surfaces were Turbo-CSL and GEWA-C. Integrally low-fin tubes had fin density of 26 fpi. The internal test section dimensions were $554 \times 650 \times 69$ mm ($W \times H \times D$). The tube pitches, center to center, were 25.5, 28.6, and 44.5 mm. Arrays of 6–10 tubes were tested for the tube diameter of 19.05 mm. The condensing heat transfer coefficient was tested at nominal heat fluxes of 20, 40, and 60 $kW/m^2$ with liquid film inundation. It was found that at small inundation rates, heat transfer coefficients of the three-dimensional enhanced tubes were higher than low-fin tubes. The increment of inundation rates deteriorated the performance of the 3D enhanced tubes, while the heat transfer coefficient of the low-fin tube was almost unchanged for inundation film Reynolds numbers from 0 to 4500. Low-fin tubes were suggested for use in the lower rows of water cooled condensers with many rows and Reynolds numbers greater than 1250.

Although the row effect for enhanced tubes was not clearly established in literature, a notable decrease in condensing heat transfer performance was observed on a large sample of enhanced tube bundles. The row effect was negligible for the low-fin tubes, which is beneficial for condensing heat transfer of shell-and-tube condensers. However, according to a systematic survey [6,22–24] of single-tube performance of condenser tubes, three-dimensional enhanced tubes typically have higher heat transfer coefficients than low-fin tubes. With advancements in machining technology, it is now possible to produce double-sided enhanced low-fin tubes with high fin density and height. The high-density low-fin enhanced tube design could have competitive, and even higher, overall heat transfer coefficient with respect to single-tube performance of 3D enhanced tubes.

As indicated above, the bundle effect plays a significant role in the performance of condensers. The effect of film condensate on the single, high-density, low-fin tube, and the performance of full-sized condensers configured with the same low-fin tubes were investigated in the present study. Single tube heat transfer performance was first tested and compared with a high-performance three-dimensional enhanced tube. The three-dimensional tube used in this study is currently used by many chiller-manufacturing companies in China. Condensing heat transfer performance of R134a and R22 in the condensers made with the low-fin and three-dimensional enhanced tubes were then tested in centrifugal and screw chillers. Condensers with the two types of enhanced tubes were both fabricated by the same domestic company with advanced manufacturing technology.

## 2 Single Tube Experiment

Systematic investigations on the single tube offered a reasonable understanding on the performance of high-density low fin tubes. It is quite useful for design and fabrication of condensers.

**2.1 Experimental Apparatus.** Condensing heat transfer on a single tube was first investigated to establish a reasonable understanding of high-density low-finned tube performance with applications in condenser design and fabrication. As shown in Fig. 1, the experimental apparatus includes the refrigerant circulation and the water cooling loops. The liquid refrigerant is charged in the boiler, where electric heaters provide heat to boil the refrigerant until it becomes a vapor. The vapor refrigerant rises to the condenser, where it condenses on fixed horizontal tubes from the cooling water loop. The refrigerant condensate returns to the boiler by gravity. Cooling water flows through the test tube and then returns to water storage tank. The condenser has an inner diameter of 147 mm and a length of 1500 mm. The entire apparatus is insulated with material made from nitrile butadiene rubber and polyvinyl chloride (a kind of human-made polymer for insulation, thermal conductivity is within 0.04 W/m·K) with a thickness of 40 mm.

To quantitatively analyze the effects of the film condensate on the condensation heat transfer of single tubes, a liquid distributor is also configured vertically in the condenser above the test tube to simulate the inundation effect of the tube bundle. The liquid distributor is a second enhanced tube with the same length as test

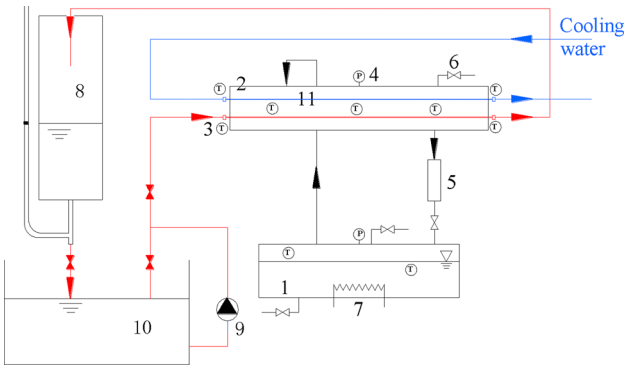


**Fig. 1 Schematic of the experimental apparatus for single tube test: 1—boiler, 2—condenser, 3—thermocouple, 4—pressure gauge, 5—condensate measuring container, 6—exhaust valve, 7—electric heater, 8—weight-time flow meter, 9—water pump, 10—water storage tank, and 11—liquid film distributors**

tube. The cooling water flows through the distributor, and the cooling power is also recorded. By controlling the heat flux of distributor, the condensate film of the refrigerant condensation on the test tube can be simulated.

The electric power for heating can be adjusted from 0 to 15 kW, and power is measured using a watt transducer with an accuracy of ±0.2%. The temperature and temperature difference of cooling water are measured using thermocouples and six-junction copper-constantan thermocouple piles. The thermocouples and thermocouple piles were calibrated against a thermometer with a precision of ±0.2 K. Five platinum resistance temperature sensors (PT100) with a precision of $\pm(0.15 + 0.002|t|)$ K were used to measure the temperatures of the refrigerant at various locations in the system. The flow rates of both cooling water circulation loops are measured with weight-time flow meters. The flow meter is a self-designed instrument. It has a vertical cylinder with a known internal diameter, where the change of liquid level over time is recorded with an optical method as the water flows into the cylinder. The overall accuracy of the weigh-time flow meter is within ±0.5% over the entire measurement range. A Keithley digital voltmeter with a resolution of ±0.1 μV is used to measure the electric potential of the sensors. A pressure gauge is used to measure the condenser pressure with the precision of ±0.00625 MPa. The test range varied from 0 to 2.5 MPa.

**2.2 Geometries of Enhanced Tube.** The condensing heat transfer of single tube experiment for the high-density low-fin tube (No. 1) and 3D enhanced tube (No. 2) was tested. Exterior surface and cross section images of the tubes are shown in Fig. 2. For the 3D enhanced surface, fin tips have been knurled in the circumferential direction. Intersected grooves can be observed outside the tube surface. Water sides were also enhanced with internal grooves. Table 1 describes the geometric parameters of each tube, where $d_o$ is the diameter of plain base tube. The integral low-fin tube has a fin density of 56 fpi and fin height of approximately 1 mm. This high-density low-finned tube was intentionally designed and was expected to have a comparable performance to any domestic, high performance, 3D enhanced tubes.

**2.3 Data Reduction.** The heat balance is examined by comparing the heat rejection rate of the cooling water and the power of the electric heaters used in the experiment.

The heat rejection through cooling water, $\phi_c$, is shown in the below equation:

$$\phi_c = m_c c_p (t_{in} - t_{out}) \tag{1}$$

where $t_{in}$ and $t_{out}$ are the inlet and outlet temperatures of cooling water (K), $c_p$ is the specific heat capacity of cooling water corresponding to the mean temperature of inlet and outlet water (J/kg·K), and $m_c$ is the mass flow rate of cooling water (kg/s). The properties of water were obtained from Ref. [25].

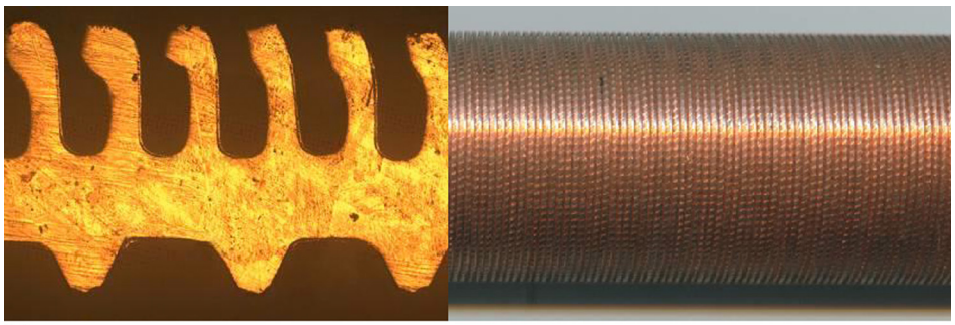

(*a*) No.1

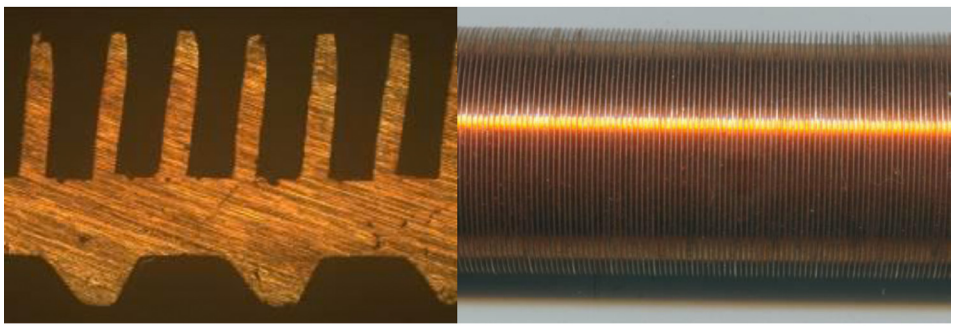

(*b*) No.2

**Fig. 2 Geometries of enhanced tubes: (*a*) No. 1 and (*b*) No. 2**

**Table 1 Specifications of tubes**

| Tubes | $d_o$ (mm) | $d_i$ (mm) | $e$ (mm) | Outside fin numbers per inch | $t$ (mm) | $L$ (mm) |
|---|---|---|---|---|---|---|
| Plain | 19.17 | 16.40 | — | — | — | 1463 |
| No. 1 | 19.04 | 16.66 | 0.981 | 43 | 0.373 | 1369 |
| No. 2 | 19.07 | 16.59 | 1.023 | 56 | 0.284 | 1464 |

The maximum difference between the heat transfer rates of cooling water and electric heaters was within 3%. The average of the two heat transfer rates is used to determine the overall heat transfer coefficient, $k$, of the single tube, with the following equation:

$$k = \frac{\phi_{avg}}{A_o \cdot \Delta t_m} \tag{2}$$

where $A_o$ is the outside surface area determined by the outside diameter of plain base tube, and $\Delta t_m$ is the log-mean temperature difference.

The condensing heat transfer coefficient, $h_o$, is obtained from the thermal resistance separation method

$$\frac{1}{k} = \frac{A_o}{A_i}\frac{1}{c_i h_i} + R_w + \frac{1}{h_o} \tag{3}$$

where $c_i h_i$ is the internal water side heat transfer coefficient. $h_i$ is the internal heat transfer coefficient of smooth tube with the same Re and physical properties as internal grooved tube, determined by Gnielinski equation [26,27]. $c_i$ is the enhanced ratio of internal grooved tube compared with smooth tube, determined by the Wilson plot technique [28,29]. Enhanced ratios of the two tubes are 2.20 and 2.73, respectively. The ratio of tube wall thermal resistance to overall thermal resistance was within 3.5% in the experiment. The effect of fin efficiency was neglected. Tube wall thermal resistance is determined by $R_w = d_o \cdot \ln(d_o/d_i)/2\lambda$.

During the experiment with upward condensate, cold water flowed through the film distributing tube. The condensate from the distributing tube fell onto the surface of test tube. The flow rate of condensate can be controlled by varying the cooling water inlet temperature and flow rate. The flow rate of condensate from the distributing tube was also measured with the weight time flow meter. As the cooling power was recorded, the amount of refrigerant condensate was determined using physical properties of the refrigerant. The effect of condensate film on the condensing heat transfer coefficient of single tube was also investigated. The film Reynolds number can be written as

$$\mathrm{Re} = \frac{4\Gamma}{\eta} \tag{4}$$

where $\Gamma$ is the total condensate draining rate from the test tube per unit tube length (kg/m·s) and was determined using the sum of heat load of the test tube and film distributing tube in the same vertical row, as shown in the below equation:

$$\Gamma = \frac{\phi_c + \phi_d}{2Lr} \tag{5}$$

where $\phi_d$ is the cooling heat transfer rate of the film distributor. $\eta$ and $r$ are the dynamic viscosity and latent heat of the condensate at the saturated state. $\Gamma$ and Re for the test tube are evaluated using the sum of condensate from the upper distributer and test tube.

Experimental uncertainty is estimated according to Refs. [30–32]. The confidence level for all measurements is 95%. The estimated uncertainty of heat flux $q(q = \phi_{avg}/A_o)$ for most data (95%) is less than 5.4%; $k$ is less than 5.6%. $h_o$ is not directly measured, and the uncertainty of $h_i$ should be within 10% for most of measurements [26,33,34]. The ratio of tube-side thermal resistance to overall thermal resistance is within 56.7%. The uncertainty of $h_o$ can be estimated using the method suggested in Ref. [15]. The uncertainty of $h_o$ for most measurements (95%) should be within ±18.7%. As show in Fig. 3, the deviation of experimental result and Nusselt analytical solution [35] is mostly within ±10%. The agreement with the analytical solution validates the experimental apparatus and procedure.

**2.4 Overall Heat Transfer Coefficient.** Figures 4(*a*) and 4(*b*) show the overall heat transfer coefficient versus the water velocity for plain and two enhanced tubes. The condensing saturation pressure was 1.01 MPa and saturation temperature was 40 °C. The heat flux was held approximately constant at 20 and 30 kW/m$^2$ by controlling the water temperature. The internal water velocity ranged from 1.5 to 2.5 m/s. Figure 5 shows the overall heat transfer coefficient of two enhanced tubes versus heat flux at a fixed water velocity 2.2±0.2 m/s. As shown in Figs. 4 and 5, the major features are as follows.

(1) The overall heat transfer coefficients of the two enhanced tubes were similar for a heat flux less than 30 kW/m$^2$. The largest deviation in heat transfer coefficient between the two enhanced tubes is 6%. The heat transfer coefficient for the enhanced tubes is approximately 7.6–9.8 times greater than that of a plain tube. At a fixed heat flux, the heat transfer coefficient increased with increasing water velocity, due to a corresponding decrease in tube-side thermal resistance. The overall heat transfer coefficient increased by about 25% as the water velocity increased from 1.5 to 2.5 m/s.

(2) The overall heat transfer coefficient decreased appreciably with the increase of heat flux for a water velocity of 2.2 m/s. The overall heat transfer coefficient varied from 10 to 14 kW/m$^2$ K for a heat flux of 10–120 kW/m$^2$. The tube-side thermal resistance was held constant, which indicates that the shell-side heat transfer coefficient contributed the most to changes in the overall heat transfer coefficient. As the film thickness outside the tube surface was increasing with increasing heat flux, the shell side condensing heat

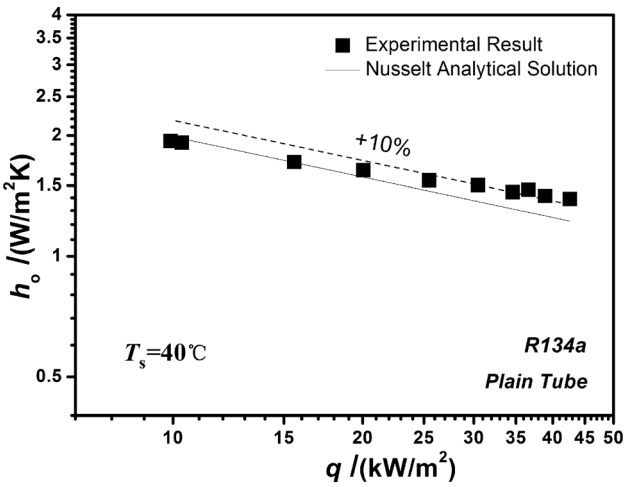


**Fig. 3 Comparison of experimental result with Nusselt analytical solution for plain tube**

transfer coefficient decreased. The rate of reduction in heat transfer coefficient became milder at higher heat fluxes.

(3) It should be noted that although the overall heat transfer coefficient looks similar, the heat transfer coefficient and thermal resistance in tube side and shell side were different for the two enhanced tubes. For a coolant velocity of 2.2 m/s and heat flux of 20 kW/m$^2$, the thermal resistance of the tube and shell side was 56.3%/40.0% and 46.4%/49.5% for the tubes No. 1 and No. 2, respectively. The shell-side thermal resistance of No. 1 was lower than that for No. 2.

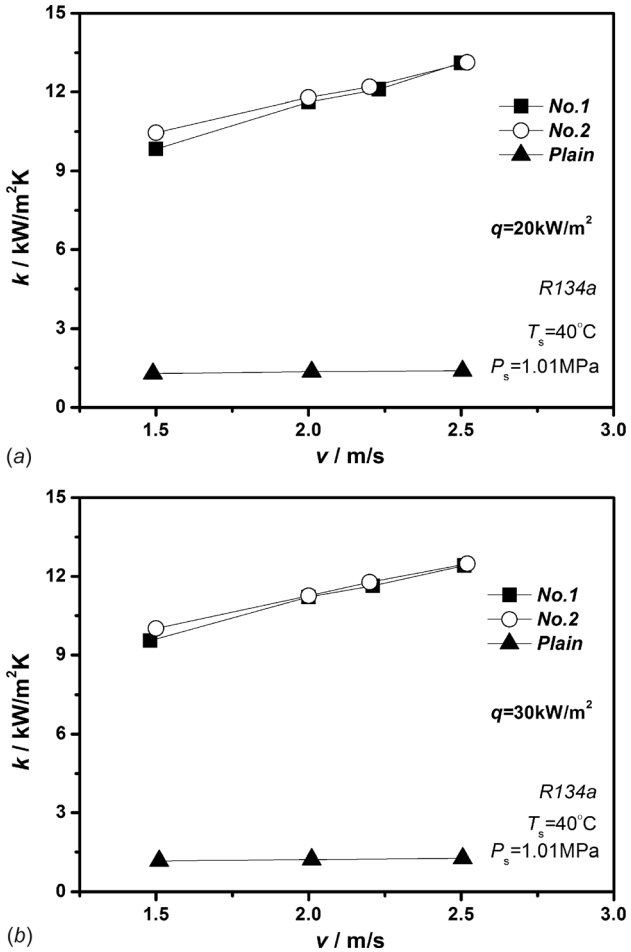


**Fig. 4 Overall heat transfer coefficient versus velocity at heat flux 20 and 30 kW/m$^2$: (*a*) heat flux=20 kW/m$^2$ and (*b*) heat flux=30 kW/m$^2$**

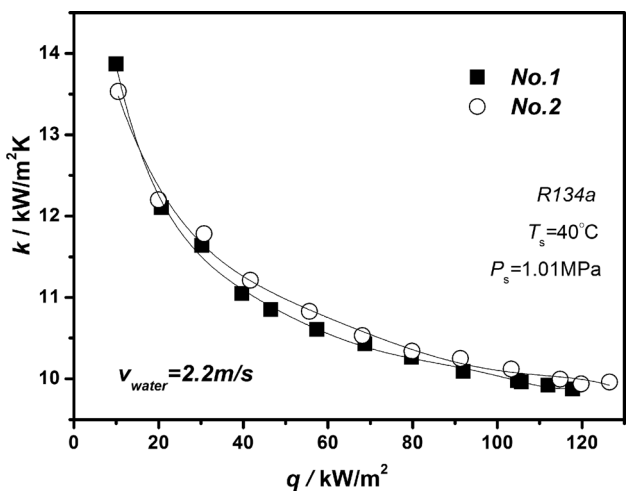


**Fig. 5 Overall heat transfer coefficient versus heat flux for No. 1 and No. 2 at internal water velocity of 2.2 m/s**

**2.5 Shell Side Condensing Heat Transfer Coefficient.** The variation of the condensing heat transfer coefficients of R134a outside the two enhanced tubes is shown in Fig. 6 as a function of heat flux. Condensing tubes with the best reported performance [6,22–24]: GEWA-C, Turbo-C, Thermoexcel-C and Turbo-CSL were also compared for a heat flux range of 0.7–126.7 kW/m$^2$. The film thickness on the tube surface increased with increasing heat flux, thereby reducing heat transfer performance. The decrease in heat transfer coefficient exhibited a nearly linear trend with the increase of heat flux in the log–log plot. The slopes of the linear best-fit for the log–log plot were −0.25 and −0.21 for No. 1 and No. 2, respectively. The heat transfer coefficient decreased by 42% when the heat flux increased from 6.7 to 46.5 kW/m$^2$.

The condensing heat transfer coefficient was between 20 and 40 kW/m$^2$ K within the test range. As shown in Fig. 6, the intentionally designed integral-fin tube No. 1 had the highest condensing heat transfer coefficient compared with other 3D enhanced tubes in the literature. The heat transfer coefficient of tube No. 2 was similar to GEWA-C and Turbo-CSL. The Thermoexcel-C tube in Zhang et al. [6] heat transfer coefficient decreased at a slower rate than the other tubes.

As indicated above, except to take full advantage of "Gregorig effect," further extending surfaces could also contribute to improving the condensing heat transfer. The external fin density of No. 1 is 56 fpi and No. 2 is 43 fpi, and the fin heights are similar. According to mathematical analysis, the heat transfer area of No. 1 was 27.7% larger than No. 2. The condensing heat transfer coefficient of No. 1 was 10.8–25.8% higher than No. 2. The comprehensive interaction of Gregorig effect and extending heat transfer area explains the physics behind the enhancement in condensing heat transfer.

**2.6 Effect of Condensate.** The effect of condensate on the condensing heat transfer of refrigerant outside the tube bundles was also an important design consideration. The effect of condensate on the shell-side condensing heat transfer for both tubes is

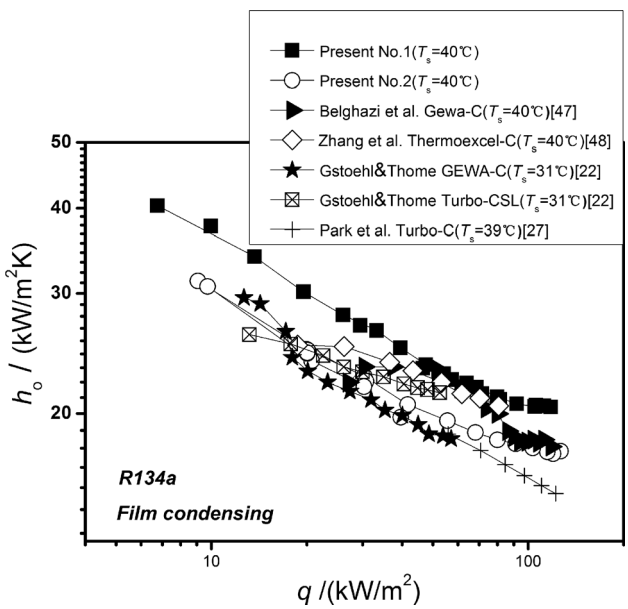


**Fig. 6 Condensing heat transfer coefficient versus heat flux for single tube**

shown in Fig. 7. Without the impinging effect from film distributor, the condensing heat transfer coefficient of tube No. 1 was 18.4% higher than that for tube No. 2. The heat transfer coefficient of No. 2 initially increased by about 20% and then decreased by 20% as film condensate Reynolds number increased from 100 to 700. It should be noted that No. 1 displayed almost no bundle effect remaining nearly constant like the overall heat transfer coefficient.

In the experiment, it was also observed that the condensate from the integral-fin tube dripped in a stable manner from a certain location in the bottom of the tube, in both droplet and column mode. However, the dripping position was moving along the axial direction on tube No. 2 (see Fig. 8) for the 3D fin profiles. Currently, there is no widely supported explanation for this phenomenon and heat transfer process in the literature. According to Webb and Murawski [17], 3D fin geometry would allow the axial spreading of condensate. A large fraction of condensate could flow longitudinally toward the ends of tube and falls downward along the tube wall. Hence, the condensate can more easily cover the surface and pass through the 3D fin profiles. For the integral finned tubes, the fin gap channels the drainage of condensate and it mostly drips from a certain location. It works like a dam, impeding the axial flow of condensate, especially for high fins. Most of the condensate remaining on the tube bottom falls vertically downward and impinges on the lower tube. The condensate drainage seems to be confined between two or more fin spaces. The effect of surface tension can reduce the condensate film thickness in the higher region of fins. The two-dimensional fins also promote circumferential condensate flow. It will increase the active heat transfer area of integral fins. When condensate impinges on the lower tubes, the heat transfer might be enhanced with impingement. The heat transfer of the low-fin tube was not influenced by the falling condensate.

## 3 Condenser Experiment

**3.1 Experimental Apparatus.** The thermal-hydraulic performance of condensers fabricated with enhanced tubes No. 1 and No. 2 was tested in the water-cooled centrifugal and screw chiller test rig. A schematic is shown in Fig. 9. R134a is used in the centrifugal chiller and R22 is used in the screw chiller.

In the evaporator of the centrifugal chiller, R134a absorbs heat from the chilled water, evaporates, and enters the centrifugal compressor as a saturated state. Driven by the centrifugal compressor, the vapor refrigerant enters the condenser at a superheated state. In the condenser, high-pressure refrigerant vapor is cooled and condensed by the cooling water. Latent heat is removed and R134a vapor changes into liquid. The liquid refrigerant passes through the subcooling section located in the bottom of the condenser to lower the refrigerant inlet temperature to the evaporator. High-pressure refrigerant liquid expands and enters the evaporator through the expansion valve. This completes the refrigerant circulation loop. Chilled and cooling water flows through the tube side of the evaporator and condenser, respectively. Since the lubricating oil can be discharged from the compressor, an oil separator is configured in the outlet of compressor. To observe the liquid level and liquid flow, sight glasses are configured in different locations of refrigeration cycle. Compressor speed can be controlled according to the experimental requirement by a frequency converter. The water flow rate and temperatures can also be controlled. The circulation loops for screw chiller are similar.

Water-cooled condensers for centrifugal chillers were fabricated with enhanced tubes No. 1 and No. 2. Tubes were mounted in the tube sheets by mechanical expansion. The supporting plates were welded in the condenser shell to prevent motion and vibration of the tube bundles. A baffle plate was used to prevent direct high-velocity impingement of vapor on the tube bundles. It was also used to promote the uniform distribution of vapor over the entire condenser. An integral subcooler was located in the bottom of condenser. It included some tubes configured in the lower region of the condenser shell, which also served as a reservoir for condensed refrigerant. In the experiment, the liquid refrigerant level was continuously monitored to provide the optimum chiller performance. The amount of flash gas formed after the expansion valve will decrease and the efficiency of chiller will increase as the degree of subcooling increases. A water baffle was located and welded within the water box to provide the required pass arrangements. A pressure relief valve set at 1.6 MPa was installed in the condenser for safety. The evaporator was a flooded-type heat exchanger. An oil filter was located outside the system in case of maintenance and replacement. The centrifugal compressor impeller was made with aluminum alloy and could be controlled according to the refrigeration load.

After the condenser was installed in the centrifugal chiller, the entire system was charged with high-pressure nitrogen to check for leaks. The pressure should be maintained for at least 24 h to ensure the whole system was well sealed. After all leaks were eliminated, the system was evacuated to an absolute pressure below 1500 Pa. The vacuum should be held for at least 30 min. Finally, refrigerant R134a was charged into the system. Polyol ester or mineral lubricant, miscible with R134a or R22, was also charged into the system to adequately lubricate the compressor. In the experiment, oil levels and oil temperature were monitored by a sight glass and sensors. The liquid level of refrigerant was recorded to make sure the charging amount was the same for each

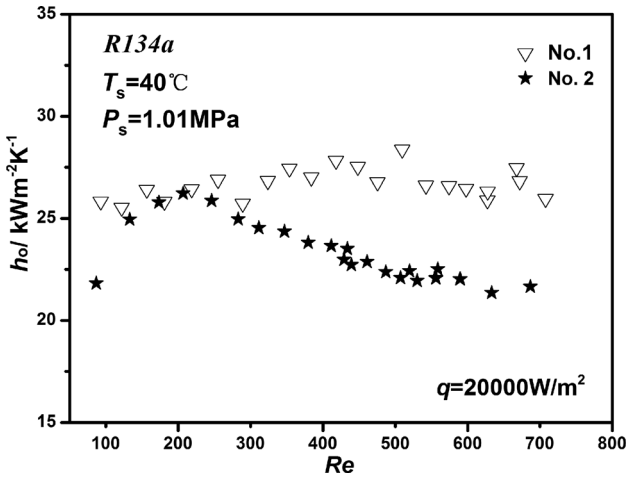


**Fig. 7 Effect of condensate Reynolds number on condensing heat transfer coefficient**

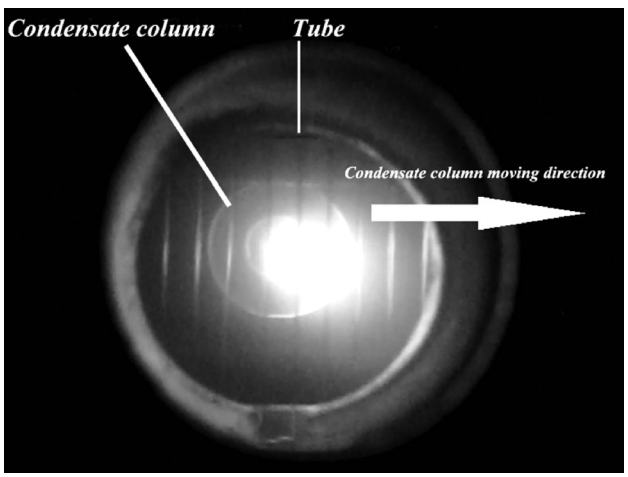


**Fig. 8 Moving direction of condensate column outside three-dimensional enhanced tubes**

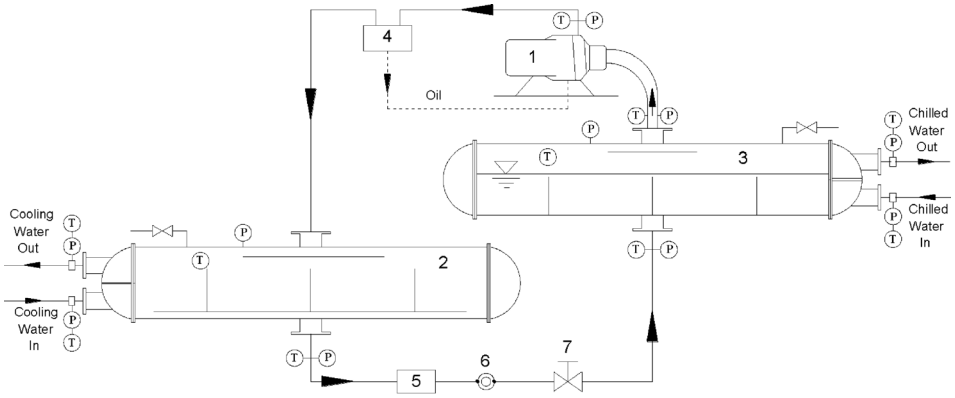


**Fig. 9 Schematic of centrifugal chiller test rig: 1—centrifugal compressor, 2—condenser, 3—evaporator, 4—oil separator, 5—dry filter, 6—sight glass, and 7—expansion valve**

test, and it was also used to roughly detect the presence of refrigerant leaks during operation.

Inlet temperatures of the chilled and cooling water could be adjusted according to the purpose of experiment. The temperature was measured with platinum resistance thermometers with an accuracy of ±0.05 °C. A power transducer is used to measure the motor power input; the precision is within ±1.25 kW. The flow rate of water is measured with an electromagnetic flow meter, which has an accuracy of ±0.5% over the entire measurement range. The full-scale accuracy of the pressure gauge for the condenser was ±0.1%.

Centrifugal chillers are commonly used in buildings where large refrigeration capacity is required. The cooling power of the condenser in this experiment could reach up to 2200 kW. Bundle effect is an important design consideration, due to the impact on thermal performance of the tubes in the condenser. Hence, the use of integral finned tubes might contribute greatly to the development of compact designs.

The screw chiller works in a manner essentially the same as centrifugal chiller. The screw chiller was also tested with condensers built from enhanced tubes No. 1 and No. 2. The refrigerant used in the screw chiller is R22. The tube bundle of the condenser for screw chiller is comprised of nine rows, whereas the condenser for the centrifugal chiller contains 18 rows. The refrigerant capacity for the screw chiller is about 650–700 kW in the typical experimental conditions, which is much lower than centrifugal chiller.

The experiment involved the determination of the refrigeration capacity of the system, coefficient of performance (COP) for the refrigeration cycle, overall heat transfer coefficients, and the shell-side condensation heat transfer coefficient. The refrigeration capacity is determined by the below equation:

$$\phi_r = m_r c_p (t_{r,in} - t_{r,out}) \tag{6}$$

The heat rejection rate of the condenser, $\phi_{cr}$, is given by

$$\phi_{cr} = m_{cr} c_p (t_{cr,in} - t_{cr,out}) \tag{7}$$

where, $t_{r,in}$ and $t_{r,out}$ are the inlet and outlet temperatures of chilled water (K). $t_{cr,in}$ and $t_{cr,out}$ are the inlet and outlet temperatures (K) of cooling water from the condenser. $c_p$ is the specific heat capacity (J/kg K) of cooling and chilled water corresponding to the mean temperature of inlet and outlet water. $m_r$ is the mass flow rate (kg/s) of chilled water flows through the flooded evaporator. $m_{cr}$ is the mass flow rate (kg/s) of cooling water flows through the condenser of chiller. The properties of water are also obtained from Ref. [25].

The heat balance between the heat rejection and refrigeration capacity is given by $\frac{(\phi_c - \phi_m) - \phi_{cr}}{\phi_{cr}}$, where $\phi_m$ is the power input of motor for compressor. The heat balance is within 2% for all cases. The overall heat transfer coefficient in condensers is determined by the below equation:

$$k_{cr} = \frac{\phi_{cr}}{A_{cr} \cdot \Delta t_{m,cr}} \tag{8}$$

The shell-side condensing heat transfer coefficient is obtained with the same thermal resistance separation method. The uncertainty analysis according to literature [30,32] has been adopted to estimate the possible uncertainty of overall and shell-side condensation heat transfer coefficient. For most of the measurements, the uncertainty of refrigeration capacity, overall heat transfer coefficient of the condensers, and shell-side condensation heat transfer coefficient are within 6.0%, 7.8%, and 21.3%, respectively.

**3.2 Parameters of Condensers.** In the present investigation, the condensers in the two chillers were retubed with low-fin tube No. 1 and 3D enhanced tube No. 2. Using the same cylindrical shell, a bundle reconstruction was performed for the condensers. It should be noted that the only component that differs in the chillers was the condenser. The evaporator, compressor, and all the other fittings are the same.

For the centrifugal condensers, the longitudinal tube pitch with No. 1 is 23 mm and transverse is 24 mm. Longitudinal pitch is 23 mm and the transverse is 20 mm for tube bundle with No. 2. For the screw condenser in screw chiller with No. 1, the transverse pitch is 22.2 mm. The longitudinal pitch is 19.24 and 25.5 mm for the upper and lower half of the cylinder, respectively. Longitudinal pitch of the tube bundle with No. 2 is 19.24 mm and the transverse is 22.2 mm. All tube bundles have a staggered layout. The condenser with No. 1 has 15% fewer tubes than that with No. 2, which is a reduction by 80 tubes for centrifugal condenser and 20 tubes for the screw condenser. The tube lengths are 4 m and 2.94 m for centrifugal and screw chiller, respectively. Subcooling section in the heat exchanger is the same for the two condensers with different types of tubes.

### 3.3 Heat Transfer Performance of Condensers

*3.3.1 Condensers for Centrifugal Chiller.* Table 2 shows the experimental parameters of the centrifugal chiller with different condensers. The tests were conducted with the same procedure and at the same operating conditions. The flow rates, motor power input, temperatures, pressures, refrigeration capacity, and COP are also presented in the table.

**Table 2 Thermal-hydraulic performances of the condensers with different enhanced tubes for centrifugal chillers**

| Item | Condenser with No. 1 | | | Condenser with No. 2 | | |
|---|---|---|---|---|---|---|
| Experimental conditions | 1 | 2 | 3 | 1 | 2 | 3 |
| Chilled water inlet temperature (°C) | 11.1 | 11.2 | 11.4 | 11.1 | 11.2 | 11.4 |
| Chilled water outlet temperature (°C) | 7.0 | 7.0 | 7.0 | 7.0 | 7.0 | 7.0 |
| Chilled water flow rate ($m^3h^{-1}$) | 362.1 | 361.8 | 362.3 | 361.8 | 362.3 | 362 |
| Cooling water inlet temperature (°C) | 32.0 | 32.0 | 30.3 | 32.0 | 32.0 | 30.0 |
| Cooling water outlet temperature (°C) | 36.2 | 36.2 | 34.5 | 36.2 | 36.2 | 34.5 |
| Cooling water flow rate ($m^3h^{-1}$) | 432.4 | 432.7 | 432.9 | 433.3 | 433.2 | 433.1 |
| Cooling water pressure drop (kPa) | 95.1 | 96.1 | 96.0 | 110.7 | 110.0 | 111.1 |
| Refrigeration capacity (kW) | 1727.5 | 1773.5 | 1842.4 | 1755.4 | 1769.4 | 1866.1 |
| Suction temperature (°C) | 5.6 | 5.6 | 5.6 | 5.6 | 6.0 | 6.8 |
| Discharge temperature (°C) | 48 | 48 | 47 | 49.4 | 49.2 | 47.2 |
| Condensing saturate temperature (°C) | 36.9 | 37.2 | 35.2 | 37.1 | 37.1 | 35.2 |
| Condenser output temperature (°C) | 36 | 36 | 34.6 | 34.4 | 34.6 | 34.4 |
| Condenser output pressure (MPa) | 0.931 | 0.931 | 0.886 | 0.929 | — | 0.888 |
| Pressure after expansion (MPa) | 0.437 | 0.434 | 0.435 | 0.432 | — | 0.437 |
| Evaporating saturation temperature (°C) | 6 | 6.3 | 5.8 | 6.1 | 5.8 | 5.7 |
| Motor power input (kW) | 402.4 | 403.5 | 404.2 | 402.4 | 402.4 | 412.6 |
| COP | 4.29 | 4.4 | 4.56 | 4.36 | 4.39 | 4.52 |

The condenser's inlet water temperature varies at different times of the year. In this experiment, the cooling water inlet temperatures were 32 and 30 °C for the centrifugal chiller, and 30 and 33 °C for the screw chiller. The inlet and outlet cooling water temperatures were measured and therefore the heat transfer rate could then be determined. The overall heat transfer coefficient was determined by Eq. (8). Figures 10 and 11 show the overall and condensing heat transfer coefficient of the two condensers at a fixed cooling water flow rate of 433 $m^3$/h and a fixed power input to the compressor. From Table 2, Figs. 10 and 11, the following features can be observed.

(1) The refrigeration capacity of the chillers built with the two different enhanced tubes and different condensers was similar. The refrigeration capacity is the net refrigeration output provided by chillers. COP indicates the refrigeration capacity under the same electric power input. COP was also similar for the chillers with different condensers. The largest difference of refrigerant capacity was within 30 kW. At the same motor power input, the deviations of COPs were within 2%. The low-fin tube condenser had the same refrigeration capacity as 3D enhanced tube while saving 15% of the material consumption.

(2) As indicated in Figs. 4, 5, 10, and 11, the average heat transfer coefficient in the condenser was much less than that for single tube. It should be noted that there are many factors that diminish the performance of condensers in chillers. These factors include the bundle inundation effect, performance of the evaporator, refrigerant charging amount, lubricant, fouling, vapor flow, liquid suction, and discharge from the compressor. For example, when a mixture of lubricant and refrigerant vapor is discharged from the compressor, a thin film of high viscosity lubricant might be formed outside the tube surface, which was proved to be detrimental to the condensing heat transfer. In the experiment, it was observed that the liquid refrigerant was occasionally discharging from the outlet of compressors. It would also degrade the performance of condensers.

From Fig. 11, it is observed that the condensing heat transfer coefficient of the condenser with No. 1 is up to 50% greater than that of No. 2. The chiller with different condensers showed a similar refrigeration capacity. While the heat transfer area of condenser with No. 2 was 25% larger than that of No. 1, the heat transfer coefficient of the condenser with No. 2 was considerably lower than that of No. 1. The heat flux of the condenser built with No. 2 was also lower. The condenser heat flux ranged from 20 to 24 kW/$m^2$ for No. 1 and 10 to 18 kW/$m^2$ for No. 2.

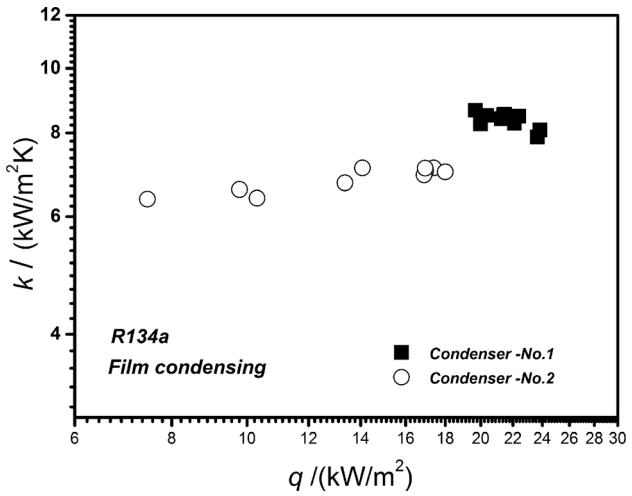


**Fig. 10 Average overall heat transfer coefficient of condensers with two enhanced tubes**

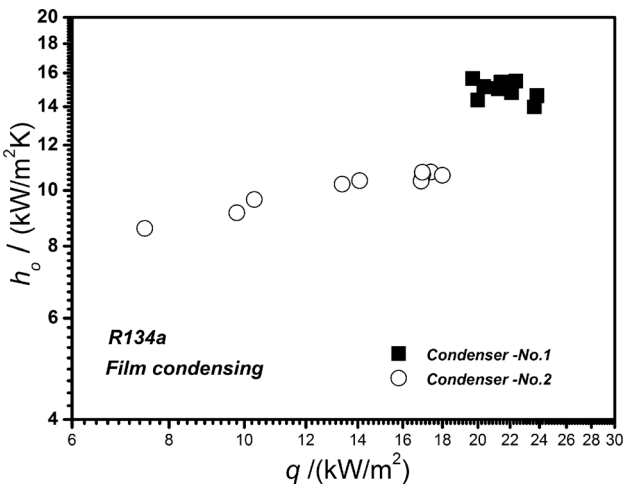


**Fig. 11 Average condensing heat transfer coefficient of condensers with two enhanced tubes**

(3) The total water side pressure drop increase that occurred in the condenser with No. 1 was 15% higher than that with No. 2. The reason was that the total flow cross-sectional area of low-fin tube condenser was 15% less than that with No. 2. The pressure drop increase was equivalent when accounting for its heat transfer area decrease. At the same cooling water flow rate of 433 $m^3$/h, the internal water velocity inside the tube of No. 1 was 2.5 m/s, and No. 2 was 2.1 m/s. Low-fin tube No. 1 had an internal fin height lower than No. 2 tube, but the internal fins per circle were three ribs more than No. 2. The pressure drop per specific length of low-fin tube No. 1 should be very close to that of No. 2 tube.

It should be noted that the refrigeration capacity was also dependent upon the performances of the compressor, evaporator, and other parts of the chiller. Replacement of the condenser could help to improve the efficiency of the system. The present results could only indicate that the condenser with low-fin tubes had the same performance as the condenser with 3D enhanced tubes.

The possible reasons to explain why high-density integral-finned tube had better heat transfer performance in the condensers were as follows: first, the condensers with such refrigeration capacity had more than 18 rows of tube bundle, and the film Reynolds number could reach up to 1700. The condensate inundation from the upward tube bundles, also possibly from the compressor, would diminish the heat transfer of the lower tube bundles. Second, the benefits of high-density low-fin tubes might help to improve the overall heat transfer performance of tube bundles. This is supported by the single tube inundation experiment [17,20–22]. Condenser designers still need to do more experiments to determine the economic benefits of using high fin density integral low-fin tubes in water-cooled shell and tube condensers.

*3.3.2 Condensers for Screw Chiller.* Table 3 shows the experimental result of screw chiller with condensers built with low-fin tube No. 1, and 3D enhanced tube No. 2. The temperatures, flow rate, motor power input, pressures, refrigeration capacity, and COP are also presented in the table. It should be noted that the refrigerant capacity for screw chiller is approximately 650–700 kW, much lower than the centrifugal chiller. The condenser in the screw chiller had nine rows in the tube, whereas the centrifugal chillers had 18 rows. The film Reynolds number was within 800, which is also considerably lower than the corresponding values for the condensers in the centrifugal chiller.

As shown in the table, the performance of screw chiller with the two different condensers was also essentially the same. The chiller with high-density low-fin tube condenser had a little bit higher COP than that for the No. 2. The internal water flow rate for the condenser with No. 1 was 4% higher than that with No. 2, which is beneficial for overall heat transfer performance. Through analysis, it was found that the overall heat transfer coefficient for low-fin tube condenser was 8.5–10.8% higher than that with 3D tube. The shell-side average condensing heat transfer coefficient for the condenser with No. 1 was 11.4–17.1% higher than that with No. 2. Both are lower than that for the centrifugal chillers.

The different refrigerants used in the chiller system, R134a and R22, might perform differently on different tubes. The inundation effect caused by the falling condensate also varies with refrigerant. The thermophysical properties of the two refrigerants differ, but neither refrigerant appeared sensitive to inundation effects in the high-density low-fin tube bundles. A 15% reduction in tube number was achieved for the condensers with high-density low-fin tubes. The tube selection had less effect on the overall performance of the chillers. Compared with the condenser with R134a, it had less tube bundles with R22. For the condensers in investigation, the heat transfer coefficient was more than 14 $kW/m^2 \cdot K$ for R134a in centrifugal chiller, and around 11 $kW/m^2 \cdot K$ for R22 in screw chiller. The condensing heat transfer coefficient of R22 might normally be higher than R134a for single tube test according to other published investigations [36,37]. The bundle effect was expected to be more significant for more tube bundles; however, the present investigation demonstrated that R134a still exhibited a higher heat transfer coefficient in the chiller. These results might indicate that the condenser in the screw chiller with R22 has potential. Other parts in the chiller, such as the evaporator, might also affect the performance of condensers. The different refrigerants were chiefly used to examine whether high-density low-finned tubes also had higher heat transfer coefficients in different chillers. The present study indicated that the high-density low-fin tube were effective and cost-competitive for both R134a and R22.

Currently, 3D enhanced tubes are extensively used in shell and tube condensers, because they exhibit the best single-tube performance. While, according to the investigations of Webb and Murawski [17], and Gstoehl and Thome [21,22], condensate inundation could significantly reduce the heat transfer performance of 3D enhanced tubes. However, the data for low fin tubes in the literature were mostly for lower fin densities within 26 fpi and lower heat transfer coefficient. One major novelty of the present paper is that a more systematic research was conducted on the performance of 56 fpi, high-density, integral-fin tubes and found that it was still effective on both single tube experiment and water-cooled condenser of large scale. The heat transfer coefficient of 3D enhanced tubes can be higher for single tube applications, but lower when installed in a large capacity condenser. High-density low finned tubes are suggested for use in the large condensers, especially in the lower rows.

A challenge of high-density low-fin tube condensers is the potential of cut-down during installation. The cut-down usually occurs in the tube supporting plates and tube sheets, which decreases the effective heat transfer area of the tubes. Scraps from the tubes might also clog the filters in the refrigerant circulation loops. Hence, it is recommended that additional protective measures are adopted in the installation process to prevent the cut-down of external fins that would degrade performance.

**Table 3 Thermal-hydraulic performances of the condensers with different enhanced tubes for screw chillers**

| Item | Condenser with No. 1 | | Condenser with No. 2 | |
|---|---|---|---|---|
| Experimental conditions | 1 | 2 | 1 | 2 |
| Cooling water inlet temperature (°C) | 30 | 32.97 | 29.97 | 32.97 |
| Cooling water outlet temperature (°C) | 33.73 | 36.93 | 33.87 | 37.13 |
| Cooling water flow rate ($m^3h^{-1}$) | 177.2 | 177.3 | 184.4 | 184.2 |
| Refrigeration capacity (kW) | 653.4 | 691.3 | 658.3 | 706.6 |
| Motor power input (kW) | 153.8 | 165.7 | 151.6 | 164 |
| Condensing pressure (bar) | 13.25 | 14.45 | 13.2 | 14.52 |
| Condenser output pressure (bar) | 13.15 | 14.2 | 12.42 | 13.5 |
| Condensing saturation temperature (°C) | 37.02 | 40.31 | 36.88 | 40.49 |
| Condenser output temperature (°C) | 33.1 | 36.1 | 31.9 | 34.4 |
| COP | 4.25 | 4.17 | 4.34 | 4.31 |

## 4 Conclusions

In this paper, high-density, low-fin tube, with a fin height greater than 1 mm, was manufactured, which was intentionally designed to have comparable performance as the high-performance 3D enhanced tubes. The overall, condensing heat transfer coefficients, and bundle inundation effect were first investigated in a single tube experiment. Then the investigation on the refrigeration capacity, tube side pressure drop, and coefficient of performance of the condensers in the centrifugal and screw chillers was conducted. The major findings are as follows:

(1) The overall heat transfer coefficient of high-density low-fin tube No. 1 and 3D enhanced tube No. 2 was quite similar in single tube experiment, and No. 1 shows almost no bundle effect.
(2) Refrigeration capacity of centrifugal and screw chillers with condensers built with low-fin tube No. 1 and 3D tube No. 2 was nearly equal. The COP was also very similar.
(3) The low-fin tube condenser for centrifugal chillers saved 80 tubes with length of 4 m and 20 tubes for the screw chiller with length of 2.94 mm when compared with 3D enhanced tubes.
(4) The low-fin tube No. 1 had higher heat transfer performance in the chillers with large refrigeration capacity. The heat transfer improvement with the low-fin tube for the condensers in centrifugal chiller was higher than that in the screw chiller.


## Funding Data

- National Key Projects of Fundamental R/D of China (973) (No. 2013CB228304).
- NNSFC (51776160).
- 111 Project (B16038).


## Nomenclature

$A$ = area, $m^2$
$c_i$ = enhanced ratio of inside heat transfer coefficient
$c_p$ = specific heat capacity, $J \cdot kg^{-1} \cdot K^{-1}$
$d$ = diameter of tube, mm
$e$ = height of outside fin, mm
$f$ = drag coefficient
$h$ = heat transfer coefficient, $W \cdot m^{-2} \cdot K^{-1}$
$k$ = overall heat transfer coefficient, $W \cdot m^{-2} \cdot K^{-1}$
$L$ = tube's test length, m
$m$ = mass flow rate, $kg \cdot s^{-1}$
$P$ = pressure, MPa
$q$ = heat flux, $kW/m^2$
$r$ = latent heat of refrigerant, kJ/kg
Re = Reynolds number
$R_w$ = thermal resistance of tube wall
$t$ = temperature, ° C; height of inside fin, mm

### Greek Symbols

$\Delta t_m$ = logarithmic mean temperature difference
$\lambda$ = thermal conductivity, $W \cdot m^{-1} \cdot K^{-1}$
$\phi$ = heat transfer rate, W

### Subscripts

avg = average
c = cooling
cr = condenser in the chiller
d = film distributing tube
i = inside of the tube
in = inlet of the tube
o = outside of the tube
out = outlet of the tube
r = refrigeration
s = saturation
w = wall

## References


[1] Webb, R. L., and Kim, N. H., 2005, *Principle of Enhanced Heat Transfer*, Taylor & Francis, Boca Raton, FL.
[2] Fernandez Seara, J., Uhia, F. J., Diz, R., and Dopazo, J. A., 2010, "Vapour Condensation of R22 Retrofit Substitutes R417A, R422A and R422D on CuNi Turbo C Tubes," Int. J. Refrig., **33**(1), pp. 148–157.
[3] Zhang, Z., Li, Q., Xu, T., Fang, X., and Gao, X., 2012, "Condensation Heat Transfer Characteristics of Zeotropic Refrigerant Mixture R407C on Single, Three-Row Petal-Shaped Finned Tubes and Helically Baffled Condenser," Appl. Therm. Eng., **39**, pp. 63–69.
[4] Ji, W.-T., Zhao, C.-Y., Zhang, D.-C., Li, Z.-Y., He, Y.-L., and Tao, W.-Q., 2014, "Condensation of R134a Outside Single Horizontal Titanium, Cupronickel (B10 and B30), Stainless Steel and Copper Tubes," Int. J. Heat Mass Transfer, **77**, pp. 194–201.
[5] Ji, W.-T., Numata, M., He, Y.-L., and Tao, W.-Q., 2015, "Nucleate Pool Boiling and Filmwise Condensation Heat Transfer of R134a on the Same Horizontal Tubes," Int. J. Heat Mass Transfer, **86**, pp. 744–754.
[6] Zhang, D. C., Ji, W. T., and Tao, W. Q., 2007, "Condensation Heat Transfer of HFC134a on Horizontal Low Thermal Conductivity Tubes," Int. Commun. Heat Mass Transfer, **34**(8), pp. 917–923.
[7] Ji, W. T., Zhang, D. C., Feng, N., Guo, J. F., Numata, M., Xi, G. N., and Tao, W. Q., 2010, "Nucleate Pool Boiling Heat Transfer of R134a and R134a-PVE Lubricant Mixtures on Smooth and Five Enhanced Tubes," ASME J. Heat Transfer, **132**(11), p. 011502.
[8] Ji, W.-T., Qu, Z.-G., Li, Z.-Y., Guo, J.-F., Zhang, D.-C., and Tao, W.-Q., 2011, "Pool Boiling Heat Transfer of R134a on Single Horizontal Tube Surfaces Sintered With Open-Celled Copper Foam," Int. J. Therm. Sci., **50**(11), pp. 2248–2255.
[9] Ji, W.-T., Li, Z.-Y., Qu, Z.-G., Guo, J.-F., Zhang, D.-C., He, Y.-L., and Tao, W.-Q., 2015, "Film Condensing Heat Transfer of R134a on Single Horizontal Tube Coated With Open Cell Copper Foam," Appl. Therm. Eng., **76**, pp. 335–343.
[10] Ji, W.-T., Jacobi, A. M., He, Y.-L., and Tao, W.-Q., 2015, "Summary and Evaluation on Single-Phase Heat Transfer Enhancement Techniques of Liquid Laminar and Turbulent Pipe Flow," Int. J. Heat Mass Transfer, **88**, pp. 735–754.
[11] Ji, W.-T., Zhao, C.-Y., Zhang, D.-C., Yoshioka, S., He, Y.-L., and Tao, W.-Q., 2016, "Effect of Vapor Flow on the Falling Film Evaporation of R134a Outside a Horizontal Tube Bundle," Int. J. Heat Mass Transfer, **92**, pp. 1171–1181.
[12] Ji, W.-T., Jacobi, A. M., He, Y.-L., and Tao, W.-Q., 2017, "Summary and Evaluation on the Heat Transfer Enhancement Techniques of Gas Laminar and Turbulent Pipe Flow," Int. J. Heat Mass Transfer, **111**, pp. 467–483.
[13] Zhao, C.-Y., Jin, P.-H., Ji, W.-T., He, Y.-L., and Tao, W.-Q., 2017, "Experimental Investigations of R134a and R123 Falling Film Evaporation on Enhanced Horizontal Tubes," Int. J. Refrig., **75**, pp. 190–203.
[14] Marto, P., 1988, "An Evaluation of Film Condensation on Horizontal Integral-Fin Tubes," ASME J. Heat Transfer, **110**(4b), pp. 1287–1305.
[15] Gregorig, R., 1954, "Film Condensation on Finely Rippled Surfaces With Consideration of Surface Tension," Z. Angew. Math. Phys., **5**, pp. 36–49.
[16] Kedzierski, M., and Webb, R., 1990, "Practical Fin Shapes for Surface-Tension-Drained Condensation," ASME J. Heat Transfer, **112**(2), pp. 479–485.
[17] Webb, R. L., and Murawski, C. G., 1990, "Row Effect for R-11 Condensation on Enhanced Tubes," ASME J. Heat Transfer, **112**(3), pp. 768–776.
[18] Al-Badri, A. R., Bär, A., Gotterbarm, A., Rausch, M. H., and Fröba, A. P., 2016, "The Influence of Fin Structure and Fin Density on the Condensation Heat Transfer of R134a on Single Finned Tubes and in Tube Bundles," Int. J. Heat Mass Transfer, **100**, pp. 582–589.
[19] Honda, H., Uchima, B., Nozu, S., Torigoe, E., and Imai, S., 1992, "Film Condensation of R-113 on Staggered Bundles of Horizontal Finned Tubes," ASME J. Heat Transfer, **114**(2), pp. 442–449.
[20] Cheng, W. Y., and Wang, C. C., 1994, "Condensation of R134a on Enhanced Tubes," ASHRAE Trans., **100**(Pt. 2), pp. 809–817.
[21] Gstoehl, D., and Thome, J., 2006, "Film Condensation of R-134a on Tube Arrays With Plain and Enhanced Surfaces—Part II: Empirical Prediction of Inundation Effects," ASME J. Heat Transfer, **128**(1), pp. 33–43.
[22] Gstoehl, D., and Thome, J., 2006, "Film Condensation of R-134a on Tube Arrays With Plain and Enhanced Surfaces—Part I: Experimental Heat Transfer Coefficients," ASME J. Heat Transfer, **128**(1), pp. 21–32.
[23] Belghazi, M., Bontemps, A., and Marvillet, C., 2002, "Filmwise Condensation of a Pure Fluid and a Binary Mixture in a Bundle of Enhanced Surface Tubes," Int. J. Therm. Sci., **41**(7), pp. 631–638.
[24] Park, K.-J., Kang, D. G., and Jung, D., 2011, "Condensation Heat Transfer Coefficients of R1234yf on Plain, Low Fin, and Turbo-C Tubes," Int. J. Refrig., **34**(1), pp. 317–321.
[25] Yang, S. M., and Tao, W. Q., 2006, *Heat Transfer*, Higher Education Press, Beijing, China.
[26] Gnielinski, V., 1976, "New Equations for Heat and Mass Transfer in Turbulent Pipe and Channel Flows," Int. J. Chem. Eng., **16**(2), pp. 359–368.
[27] Ji, W. T., Zhang, D. C., He, Y. L., and Tao, W. Q., 2011, "Prediction of Fully Developed Turbulent Heat Transfer of Internal Helically Ribbed Tubes—An Extension of Gnielinski Equation," Int. J. Heat Mass Transfer, **55**(4), pp. 1375–1384.

[28] Rose, J. W., 2004, "Heat-Transfer Coefficients, Wilson Plots and Accuracy of Thermal Measurements," Exp. Therm. Fluid Sci., **28**(2–3), pp. 77–86.
[29] Ji, W.-T., Zhao, C.-Y., Zhang, D.-C., He, Y.-L., and Tao, W.-Q., 2012, "Influence of Condensate Inundation on Heat Transfer of R134a Condensing on Three Dimensional Enhanced Tubes and Integral-Fin Tubes With High Fin Density," Appl. Therm. Eng., **38**, pp. 151–159.
[30] Kline, S. J., and Mcclintock, F. A., 1953, "Describing Uncertainties in Single-Sample Experiments," Mech. Eng., **75**(7), pp. 3–9.
[31] Moffat, R. J., 1988, "Describing the Uncertainties in Experimental Results," Exp. Therm. Fluid Sci., 1(1), pp. 3–17.
[32] Cheng, B., and Tao, W. Q., 1994, "Experimental Study of R-152a Film Condensation on Single Horizontal Smooth Tube and Enhanced Tubes," ASME J. Heat Transfer, **116**(1), pp. 266–270.
[33] Cengel, Y. A., and Ghajar, A. J., 2011, *Heat Mass Transfer*, McGraw-Hill, New York.
[34] Incropera, F. P., DeWitt, D. P., Bergman, T. L., and Lavine, A. S., 2011, *Fundamentals of Heat and Mass Transfer*, Wiley, New York.
[35] Nusselt, W., 1916, "Die oberflachencondensation des wasserdampfes," VDI, **60**, pp. 541–569.
[36] Jung, D., Kim, C.-B., Hwang, S.-M., and Kim, K.-K., 2003, "Condensation Heat Transfer Coefficients of R22, R407C, and R410A on a Horizontal Plain, Low Fin, and Turbo-C Tubes," Int. J. Refrig., **26**(4), pp. 485–491.
[37] Park, K.-J., and Jung, D., 2007, "Condensation Heat Transfer Coefficients of HCFC22, R410A, R407C and HFC134a at Various Temperatures on a Plain Horizontal Tube," J. Mech. Sci. Technol., **21**(5), pp. 804–813.